Monitoring of hysteretic friction degradation of Curved Surface Sliders through a nonlinear constrained estimator

A. Calabrese[1], E. Gandelli[2], V. Quaglini[2], S. Strano[3,*], M. Terzo[3], C. Tordela[3]

[1]*Civil Engineering and Construction Engineering Management (CECEM), California State University, Long Beach, CA, USA.*

[2] *Politecnico di Milano, Department of Architecture, Built Environment and Construction Engineering, 20133, Milan, Italy.*

[3]*Department of Industrial Engineering, University of Naples Federico II, Naples, Italy.*

[*]*corresponding author: salvatore.strano@unina.it*

Abstract

The lack of validated physical models concerning the degradation of the coefficient of friction of sliding isolators induced from the heating of the sliding surfaces during the seismic motion hampers the interpretation of experimental data and the formulation of accurate numerical models. An estimator based on a Constrained Unscented Kalman Filter (CUKF), suitable for real-time monitoring, combined with a Random Walk Model approach (RWM) which identifies the friction degradation function without the a priori knowledge of a physical model and ensuing analytical law has been developed in the study. Both numerical analyses and experimental tests of a 2 DOF shear-type physical model are employed to demonstrate the validity of the technique. The proposed estimator is able to provide an accurate estimation of the state of the system, by predicting the structural displacement histories, and to identify the hysteretic degradation function in different friction conditions, from low to high friction.

Keywords: sliding isolators, model-based estimator, health monitoring, nonlinear constrained estimation, coefficient of friction, hysteretic degradation

1. Introduction

Since the early ´90s of the last century, sliding bearings with curved surfaces, known in North America as Friction Pendulum System (FPS) [1,2], and in Europe as Curved Surface Slider (CSS) [3,4], have been implemented in base isolation systems of buildings, bridges and industrial facilities, in a large number of countries worldwide [5].

A key parameter governing the dynamic behavior of CSSs is the coefficient of friction of the sliding surfaces. The coefficient of friction determines the effective stiffness, and hence the maximum force of the isolator, and the effective damping, which controls the maximum displacement during an earthquake [6]. Additionally, the influence of an initial offset, that can be caused by thermal loads or foreshock seismic events, on the recentring capability as well as on the maximum displacement of structures implementing CSS isolators has been also investigated in both experimental [3, 7-8] and numerical studies [4]. A fair prediction of the peak displacement of CSS isolators under the design seismic scenario is a crucial task for structural engineers since it was proven that, although quite unlikely, the structural collapse may mainly occur due to the overcoming of their displacement capacity [9-11]; a risk that must be prevented according to Eurocode 8 provisions [12-13]. In this regard, to define the dissipative behavior of sliding bearings is not trivial since the actual coefficient of friction is in turn influenced from a number of factors, including the instantaneous values of pressure and velocity at the sliding surfaces, the temperature, the wear and contamination of the surfaces, and the distance travelled during the seismic motion [14]. In this regard, experimental and numerical studies reported indeed that deterioration of the coefficient of friction occurs during cyclic motion of the isolator [15 – 17]: during sliding, the seismic energy introduced in the system is dissipated as heat through friction (this mechanism is hence called as “hysteretic heating”), producing a rise in temperature at the sliding interface, which in turn causes a decrease in the friction coefficient [15,18 – 20]. Numerical investigations [16,21,22] indeed demonstrated that ignoring the temperature dependence of the friction coefficient can lead to a considerable overestimation of the isolator’s damping capability.

By accounting for this mechanism, the coefficient of friction of the CSSs can be formulated as the product of two independent functions [14,22]:

$$\mu(N,V,c) = \mu_{NV}(N,V) \cdot f_c(c) \quad (1)$$

where $\mu_{NV}(N,V)$ is a first function that accounts for the dependence on the instantaneous values of axial load N and velocity V (suitable expressions have been proposed by e.g. [22]) and $f_c(c)$ is the degradation function that accounts for the variation of the coefficient of friction during the motion

due to hysteretic heating.

A suitable expression for the degradation function was proposed by Lomiento [14] based on cyclic tests of isolators performed at the CALTRANS SMRD laboratory

$$f_C(c) = e^{-\left(\left(\frac{c}{c_{ref}}\right)^{\gamma}\right)} \quad (2)$$

where the c_{ref} is a parameter that regulates the rate of degradation, γ is a parameter that controls the shape of the function, and c is a degradation variable defined by Eq. (3):

$$c(t) = \int_0^t N(t)V(t)^2 dt \quad (3)$$

By the above formulation, the change of the friction coefficient induced by hysteretic heating is related to the cumulated power dissipated at the sliding surface and the distance traveled by the slider. It is worth noting that, although Eq. (2) was originally formulated based on the results of unidirectional tests, its suitability for bidirectional movements has been proven in a dedicated study [12]. It has been indeed demonstrated that the temperature rise of the sliding surface is strongly affected by the trajectory of motion of the slider [16,23,24]. Moreover, due to the complexity of the problem and the number of variables involved, like the trajectory of motion, the materials and relevant thermal conductivity, and the size of the sliding surface in relation to the amplitude of motion [15,16], validated expressions for the degradation function f_c are still missing in practice. In agreement with the simplified design approach provided in modern seismic codes like e.g., the ASCE /SEI7-16 [25], the EC8-part 2 [13], and the AASHTO "Guide Specification for Seismic Isolation Design" [26], structural engineers have to perform upper and lower bound analyses to guarantee a robust design of the isolation system accounting for the variation of the properties of the isolators occurring in real applications on a project-specific and product-specific basis. The main assumption behind this approach is that in-service properties will be constrained between an upper bound and a lower bound limit, which are linked to the design (mean) value of each property through suitable property modification factors, or λ factors. For the particular case of sliding isolators, the European standard on antiseismic devices EN 15129 [27] assumes three factors responsible for property variation, namely ambient temperature and service life; aging; and production variability. The variation associated with the first two factors is determined from standardized prototype tests, while for production variability a ±20% maximum deviation from the design value is recommended. The North American codes AASHTO [26] and ASCE/SEI [25] also account for the variability of the isolator's performance by means of lower and upper bound analyses. For sliding systems, AASHTO [26] introduces λ factors to account for the distinct effects of temperature, aging and corrosion, velocity,

accumulated travel, and contamination. In the latest edition, ASCE-SEI [25] provides a systematic procedure for establishing upper and lower boundary values for isolator properties with consideration, in addition to aging, environmental conditions, and manufacturing variability, of the effects of hysteretic heating and history of loading. Eventually, when experimental data are missing, all standards provide de facto values for likely variations due to each category of effects for use in design.

However, the difficulty in determining appropriate values for the lambda factors from experiments is one of the limitations of using bounding analysis. Sources of variability in the performance of devices may occur simultaneously in standardized tests, influencing each other. The lack of established theoretical models, like in the case of the hysteretic degradation of the coefficient of friction, makes difficult the analysis of the experimental data to identify the contribution of each source of variability. Therefore, the definition of an individual lambda factor for each source of variability turns out to be controversial and dependent on engineering judgment. Moreover, with the advancements in the technology and the introduction of novel materials and design solutions into modern isolators, new sources of variation are disclosed from prototype tests. Since the introduction of property modification factors, the availability of new experimental results from extensive testing programs has been constantly used to update upper and lower bound values. As a result, a general agreement on the definition of reliable modification factors that can be safely used for the design has not yet been achieved.

In this regard, this study presents a novel tool to estimate the degradation of the friction coefficient due to the hysteretic heating. The tool is based on the employment of a constrained unscented Kalman filter (CUKF) integrated with a Random Walk model [28 – 36] for the degradation function estimation. The CUKF allows to takes into account the upper and lower constraints that characterize the degradation function. The possibility to apply state constraints through this estimator, makes the estimation more accurate than the other available forms of the Kalman filter, as proven in other application fields [28 – 30].

The main advantage of the proposed estimator is the ability to perform a direct evaluation of the hysteretic degradation of the coefficient of friction without being bound to fit any *a priori* assigned physical model of f_C. The theoretical development and the formulation of a benchmark model-based estimator for shear-type frames subjected to ground accelerations are presented in Sections 2 of the paper. The algorithm is assessed in Section 3 by comparing the estimation of the degradation function f_C to the actual value provided in numerical simulations, and then it is used in Section 4 to estimate the degradation occurring during shake-table tests carried out on a base-isolated case-study frame. Eventually Section 6 provides a discussion and the general conclusions of the study.

2. Observer design model

The model-based estimator is designed through the development of a shear-type structure model with two degrees of freedom (Fig. 1). The system is composed of two lumped masses that represent the mass of the base and top of the frame, respectively. Between the base and the ground, a set of sliding isolators is interposed.

The equation of motion of the isolated structure, subjected to a ground acceleration $\ddot{u}_g$ are:

$$m_b\ddot{v}_b + c_s(\dot{v}_b - \dot{v}_t) + k_s(v_b - v_t) = -m_b\ddot{u}_g - n_iF_i$$

$$m_t\ddot{v}_t + c_s(\dot{v}_t - \dot{v}_b) + k_s(v_t - v_b) = -m_t\ddot{u}_g \quad (4)$$

where m_b is the base mass, m_t is the top mass, k_s is the elastic stiffness of the frame, c_s is the structural damping of the frame, v_b and v_t are the relative displacements of the base mass and of the top mass with respect to the ground, $\dot{v}_b$ and $\dot{v}_t$ are the relative velocities, and $\ddot{v}_b$ and $\ddot{v}_t$ are the relative accelerations of the two masses, respectively. F_i is the reaction force of a single isolator, and n_i is the number of devices [37 – 39].

The reaction force F_i of the individual isolator can be particularized to the case of sliding bearings with curved surfaces by adopting the following expression:

$$F_i = \frac{W}{R_c}v_b + \mu_{fun}Wtanh(10 \cdot \dot{v}_b) \quad (5)$$

where W is the axial load acting on the isolator, R_c is the radius of curvature of the concave surface and $\mu_{fun} = \mu_{NV} \cdot f_c$ is the coefficient of friction according to Eq. (1); f_{NV} is the load- and velocity-dependent coefficient of friction, which is assumed to be assigned, and f_c represents the hysteretic degradation function to be identified. The random walk model (RWM) technique [28,30,36] is employed to estimate the degradation function without using an *a priori* assigned analytical representation of f_c. The RWM is characterized by a stochastic dynamic model on the degradation function and on his first-time derivative:

$$\begin{bmatrix}\dot{f}_{cd}\\ \dot{f}_c\end{bmatrix} = \begin{bmatrix}0 & 0\\ 1 & 0\end{bmatrix}\begin{bmatrix}f_{cd}\\ f_c\end{bmatrix} + \boldsymbol{w}_f \quad (6)$$

where f_c represents the degradation function, f_{cd} its first-time derivative, and $\boldsymbol{w}_f$ is the random white noise. $\dot{f}_{cd}$ and $\dot{f}_c$, are the first-time derivative of f_{cd} and f_c, respectively.

Adopting the augmented state technique [37] to add f_c and its first-time derivative f_{cd} to other state variables and combining the equation (4) and (5), the complete estimator design model in continuous time form is obtained:

$$\begin{cases} m_b\ddot{v}_b = -c_s(\dot{v}_b - \dot{v}_t) - k_s(v_b - v_t) - n_i\frac{W}{R_c}v_b - n_i\mu_{fun}Wtanh(10\cdot\dot{v}_b) - m_b\ddot{u}_g \\ m_t\ddot{v}_t = -c_s(\dot{v}_t - \dot{v}_b) - k_s(v_t - v_b) - m_t\ddot{u}_g \\ \dot{f}_{cd} = 0 \\ \dot{f}_c = f_{cd} \end{cases} \quad (7)$$

So, the augmented state is given by:

$$\boldsymbol{x} = [\dot{v}_b, v_b, \dot{v}_t, v_t, f_{cd}, f_c]^T = [x_1, x_2, x_3, x_4, x_5, x_6]^T \quad (8)$$

The state space equation in discrete form is formulated by integrating the system equation (7) from time t_k to time t_{k+1}, and can be written as follows:

$$\boldsymbol{x}_{k+1} = \boldsymbol{f}(\boldsymbol{x}_k) + \boldsymbol{w}_k = \begin{bmatrix} x_{1,k} + \frac{\Delta t}{m_b}\left(-m_b u - c_s(x_{1,k} - x_{3,k}) - k_s(x_{2,k} - x_{4,k}) - F_{tot}\right) \\ x_{2,k} + x_{1,k}\Delta t \\ x_{3,k} + \frac{\Delta t}{m_t}\left(-m_t u - c_s(x_{3,k} - x_{1,k}) - k_s(x_{4,k} - x_{2,k})\right) \\ x_{4,k} + x_{3,k}\Delta t \\ x_{5,k} \\ x_{6,k} + x_{5,k}\Delta t \end{bmatrix} + \boldsymbol{w}_k \quad (9)$$

where:

$$F_{tot} = n_i W\left(\frac{x_{2,k}}{R} + \mu_{fun}tanh(10\cdot x_{1,k})\right)$$

$$\mu_{NV} = \mu_{HV} - (\mu_{HV} - \mu_{LV})exp(-\alpha_{dyn}|x_{1,k}|) + (\mu_B - \mu_{LV})exp(-\alpha_{st}|x_{1,k}|) \quad (10)$$

$$\mu_{fun} = \mu_{NV}x_{6,k}$$

$u = \ddot{u}_g$ is the imposed ground acceleration and $\boldsymbol{w}$ is the additive process noise.

The state observer is alimented by the measurement of the relative base displacement. The measurement equation can be written as follows:

$$y_{k+1} = h(x_{k+1}) + v_{k+1} = x_{2,k} + x_{1,k}\Delta t + v_{k+1} \quad (11)$$

where a measurement noise v has been added.

3. Numerical simulations

The dynamic response of the benchmark shear-type structure shown in Figure 1 to a ground motion history was simulated in a custom version of the software program for structural analysis OpenSees FEM [40], by using the *CCSBearing_BVNC* element to represent the hysteretic force-displacement behaviour of CSS isolators [22]. The *TwoNodeLink* element, available in the libraries of the software program [41], is adopted to simulate the behaviour of the frame. A very stiff elastic response is assigned to both the axial and rotational degrees of freedom ($k_a = k_t \to +\infty$) while the *ViscousDamper* material, characterized by an inherent elastic stiffness k_s and damping coefficient c_s, is adopted for lateral behaviour of the frame (shear degree of freedom). In the *CCSBearing_BVNC* element the coefficient of friction is formulated in accordance with Eq. (1), where; the hysteretic degradation of the coefficient of friction is modelled in accordance with Eqs. (2) and (3), while the instantaneous value of the coefficient of friction is given by

$$\mu_{NV} = \mu_{HV} - [\mu_{HV} - \mu_{LV}] \cdot e^{(-\alpha_{dyn} \cdot |V|)} + [\mu_B - \mu_{LV}] \cdot e^{(-\alpha_{St} \cdot |V|)} \quad (12)$$

where μ_B is the static coefficient of friction at the breakaway, μ_{LV} and μ_{HV} are the kinetic coefficients of friction at low velocity and high velocity, respectively, α_{dyn} is a parameter that governs the rate of change of the kinetic coefficient of friction with the sliding velocity, and α_{St} regulates the coefficient of friction during the transition from the sticking to the sliding condition.

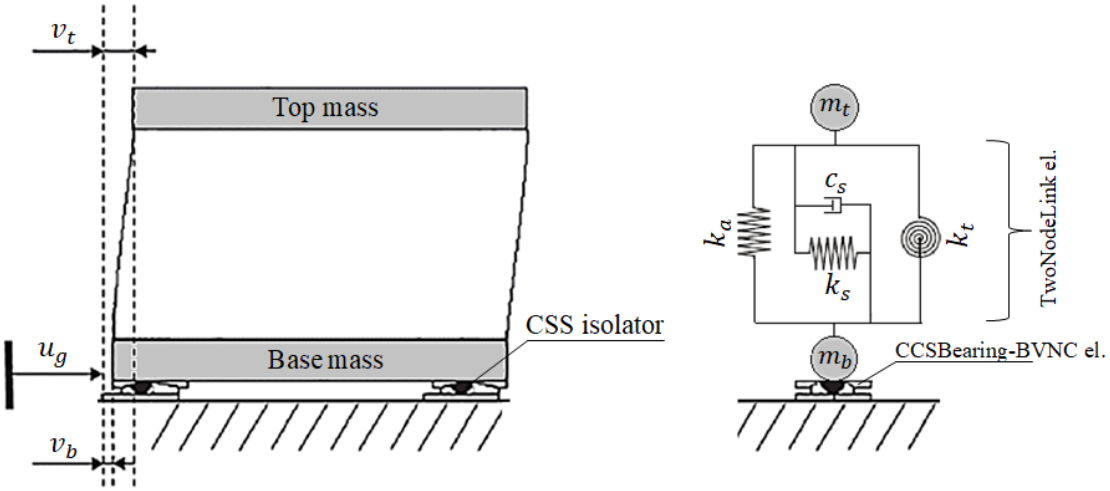


Fig. 1 Shear-type benchmark structure (left) and relevant numerical model (right)

The vertical component of the ground motion, as well as the rocking of the structure, were neglected, and hence the influence of the axial load was disregarded. The frictional parameters ()

The model parameters assumed for the Numerical_test are listed in Table 1. A dedicated procedure for the calibration of the seven constitutive parameters, five (μ_B, μ_{LV}, μ_{HV}, α_{dyn}, and α_{St}) for the dependence of the friction on the sliding velocity and two (c_{ref}, and γ) for the "frictional heating effect", is available in [22]. Since the degradation of the friction coefficient depends on the heating

power compared to the thermal mass of the steel backing plates [14], experimental force-displacement data obtained from experimental tests on full-scale CSS prototypes are needed for this purpose. However, since in this section the target is to assess the effectiveness of the CUKF estimator without being representative of any real isolation system, fictitious, although reasonable, frictional parameters have been assumed.

This test aimed at demonstrating that the CUKF is able to identify the hysteretic degradation function, employing the RWM approach, by comparing the estimated states v_b, v_t and f_c to the computed nonlinear dynamic response of the structure model. The assumed ground motion acceleration history was the Chi – Chi waveform, with PGA scaled to $3\frac{m}{s^2}$, Figure 2. The analytical formulation of f_{NV} in Eq. (30) was assumed for the estimator model, with relevant parameters as per Table 1.

The initial conditions vector of the estimated states is set to $\boldsymbol{x} = [0,0,0,0,0,1]^T$ and the upper constraints are $\boldsymbol{x_U} = [\infty, \infty, \infty, \infty, \infty, 1]$ while the lower constraints are $\boldsymbol{x_L} = [-\infty, -\infty, -\infty, -\infty, -\infty, 0]$. The process noise covariance and measurement covariance matrices were assumed as $\boldsymbol{Q} = diag(10^{-10}, 0.3 \cdot 10^{-10}, 10^{-10}, 0.5 \cdot 10^{-10}, 10^{-12}, 10^{-8})$ and $R = 10^{-16}$, respectively, where $diag(\cdot, \cdot, \dots, \cdot)$ represents a matrix having non-zero elements only on its diagonal, while all other elements are null.

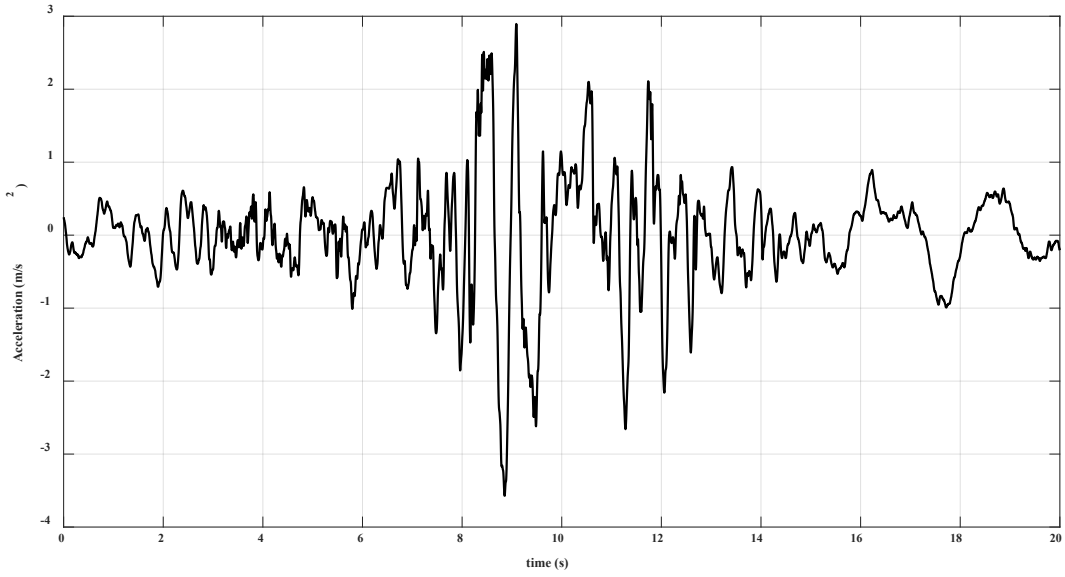
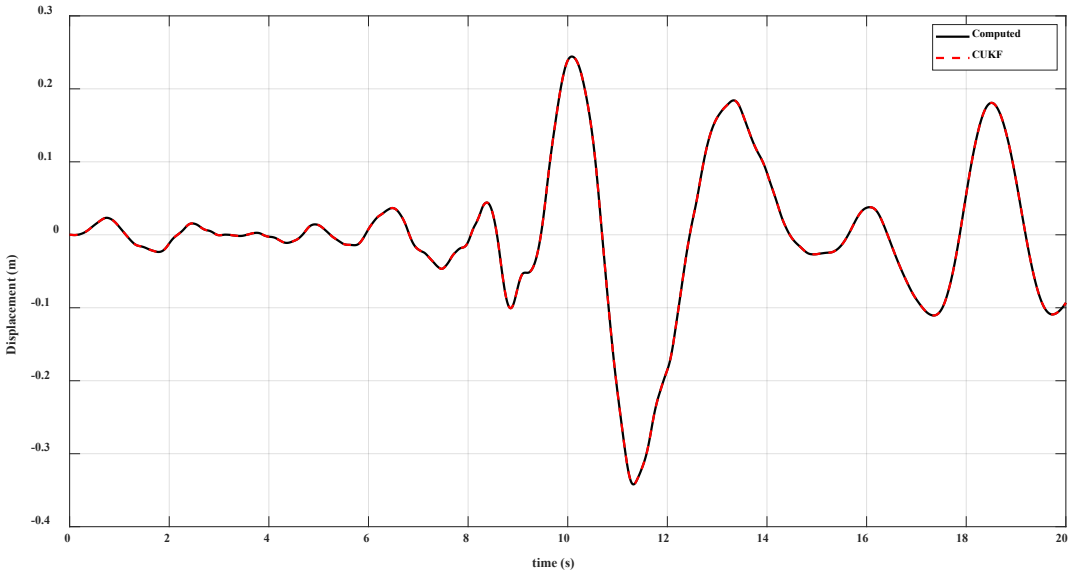
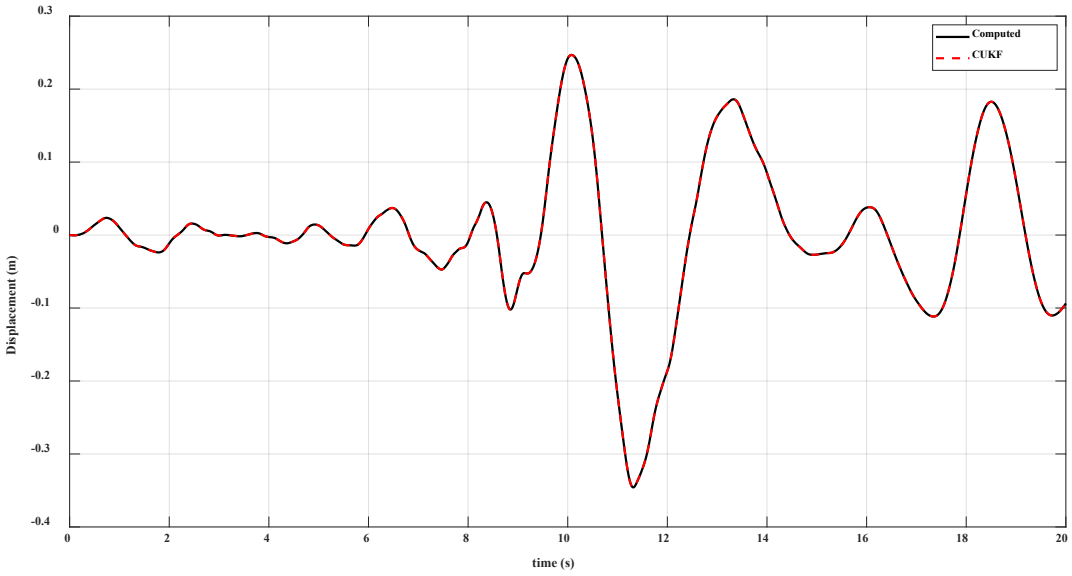


Figure 2. Chi – Chi ground ground motion acceleration history

The comparison between the estimation of the displacements at base and top levels provided by the CUKF and the computed dynamic response of the structure model from nonlinear analyses is shown in Figure 3.



(a)



(b)

Figure 3. Numerical_Test: Estimation of structure base (a) and top (b) displacement

The estimated base and top displacements are practically superimposed to the computed values. The maximum values of the estimation error relative to the structure base and top displacements are $4 \cdot 10^{-8}$ m and $5 \cdot 10^{-5}$ m respectively, demonstrating an excellent estimation quality.

Figure 4 illustrates the estimation of the hysteretic friction degradation calculated from the Random Walk Model technique. In the diagram three phases can be disclosed, corresponding to as many stages of the ground motion signal. The first phase, up to approximately 8.5 s, represents the initial stage of the ground motion, when the isolators are subjected to very small oscillations around their equilibrium

configuration. In this phase the velocity and the displacement at the sliding surfaces are very small and the friction degradation is practically negligible. The second phase, from 8.5 s to approximately 12 s, corresponds to the strong motion stage of the ground motion. The isolators are subjected to large displacements (Figure 3(a)) and high velocities, involving dissipation of seismic energy, and hence a certain degradation of the coefficient of friction. As noted from Figure 4, the predictive capability of the CUKF estimator is very fair, with only very small deviations (relative error less than 3%) from the calculated degradation history. Eventually, the third phase, from 12 s to 20 s, corresponds to the coda stage of the ground motion; the isolators have rather slow movements around their equilibrium configuration. In this last stage the rate of friction degradation becomes small, and this behaviour is correctly captured by the CUKF. In conclusion, over the whole ground motion history, the assigned hysteretic degradation function computed analytically by direct integration of the velocity history according to Eqs. (2) and (3) is correctly followed by the CUKF. The RWM technique, employed to estimate the friction degradation function, provides a reliable identification of the function.

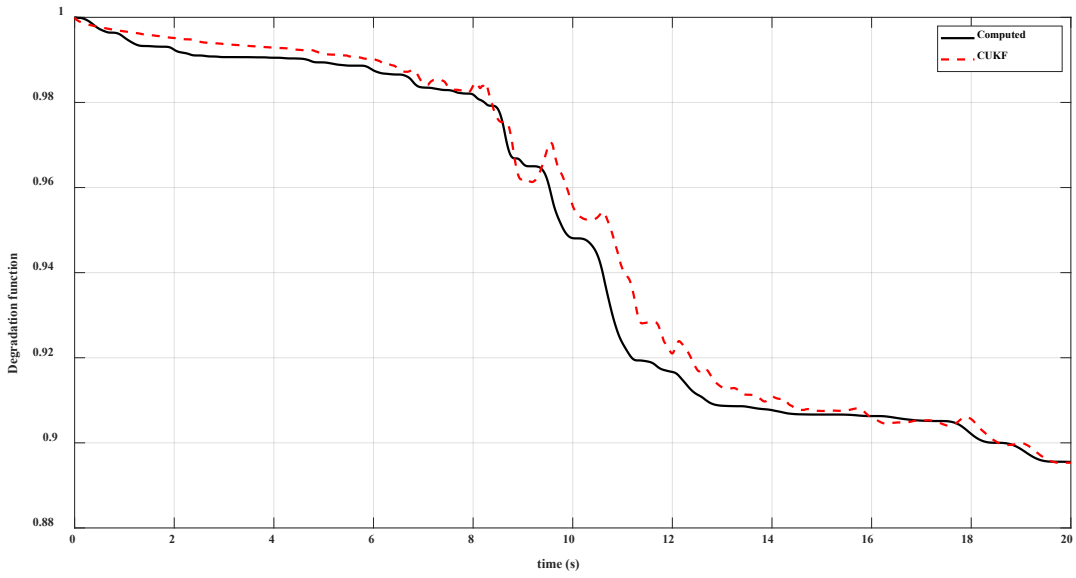


Figure 4. Numerical_Test: Comparison between estimated and assumed degradation function

Parameter	Unit	Value	OpenSees model	CUKF
m_b	Kg	20000	✓	✓
m_t	Kg	80000	✓	✓
k_s	N/m	28030000	✓	✓
c_s	Ns/m	759000	✓	✓

R_c	m	3	✓	✓
n_i	-	2	✓	✓
μ_B	-	0.14	✓	✓
μ_{HV}	-	0.032	✓	✓
μ_{LV}	-	0.008	✓	✓
α_{dyn}	s/m	15	✓	✓
α_{St}	s/m	250	✓	✓
c_{ref}	Nm^2/s	40000000	✓	×
γ	-	0.50	✓	×

Table 1. Model parameters – Numerical_Test.

The parameters c_{ref} and γ shown in Table 1 are employed only in the analytical formulation of the degradation function (Eq. (2)) that characterizes the OpenSees structure model; the other parameters are used for both the observer design model and the OpenSees model.

4. Experimental assessment

In this Section, the suitability of the proposed tool (CUKF and RWM technique) as a fair estimator of the hysterical degradation of the coefficient of friction of CSSs is assessed by exploiting the results of shaking table tests on a base-isolated case-study mock-up [3,4,30], consisting of a single-storey frame (Figure 6(a)) with in-plan dimensions of 2.65 × 2.15 m (length × width), height of 2.90 m, and a total mass of 8.2 tons examined. The fundamental mode damping was taken as 0.6%. The frame was isolated from the shake table by four CSSs inserted below the base, one isolator in correspondence of each column.

Laser displacement sensors and tri-axial piezoelectric accelerometers were used to measure the displacement and the acceleration of the superstructure at base and top levels, and two additional sensors were used to measure the displacement and the acceleration of the shake table, Figure 6(b). More details on the instrumentation and the test set-up can be found in [42].

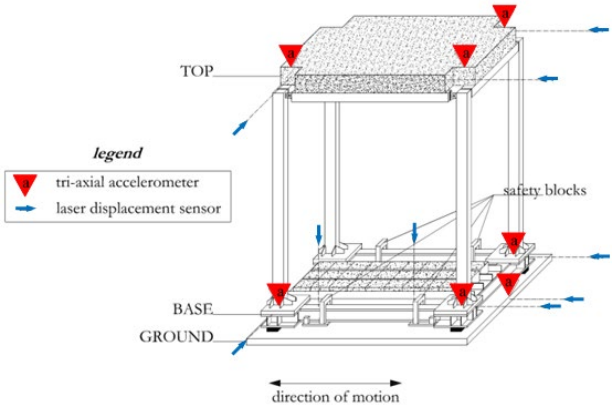
a)  b) 

Figure 5. Test set-up: case-study frame (a); layout of the instrumentation set-up (b).

The Curved Surface Slider (CSS) isolators (Figure 6), designed to fit the one-third scale mock-up, consisted of an upper and a lower sliding plate with the same radius of curvature $R_1 = R_2 = 770$ mm, and a rigid slider with height $h = 55$ mm, providing an effective radius $R_c = R_1 + R_2 - h = 1485$ mm [43]. The diameter of the sliding pads was $D = 60$ mm and the horizontal projection of the concave sliding surface was 320 mm, resulting in a displacement capacity of 260 mm.

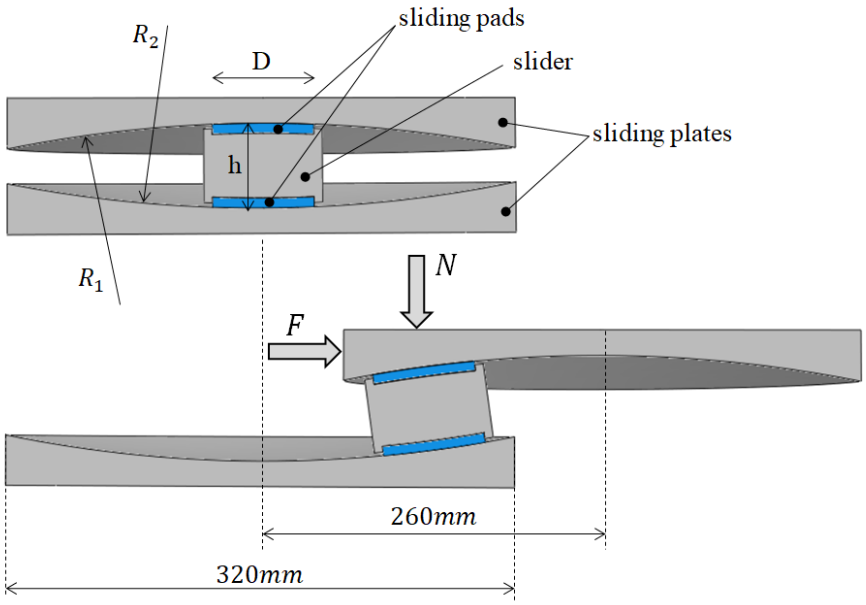


Figure 6. Curved Surface Sliders used in the experiments

The pivot and the sliding plates were made of S355 structural steel and the two concave sliding surfaces were lined with a 2.5 mm thick stainless-steel sheet. In the tests the CSS units were alternatively equipped with either high-friction (HF) or low-friction (LF) sliding pads, made of PTFE (polytetrafluoroethylene) with metal fillers, or unfilled PTFE, lubricated with silicon grease, respectively.

Based on the different friction coefficients reported in Table 2 [3,4], the two sliding materials were expected to provide dissimilar damping capacities and hence different hysteretic heating effects. In this regard, it is worth noting that the five parameters governing the "velocity effect" (μ_B, μ_{LV}, μ_{HV}, α_{dyn}, and α_{St}) of both LH and HF sliding material were defined trough small-scale tests conducted at the laboratory of Politecnico di Milano in accordance with the experimental procedure described elsewhere [44]. Four experimental datasets were considered for assessing the CUKF estimator:

1) two datasets relevant to sine-sweep tests carried out in high (HF_SSW_Test) and low (LF_SSW_Test) friction condition;
2) two datasets obtained by simulating the "Campano-Lucano" earthquake (Waveform ID 287ya from the European Strong Motion Database [45]), in high (HF_CAM_Test) and low (LF_CAM_Test) friction condition. [3,4].

The test inputs were applied to the shake table in the direction of the maximum span of the frame. Specifically, in sine sweep tests, a sinusoidal displacement with constant amplitude of 0.3 m and increasing frequency, from either 0.3 to 1.0 Hz (LF_SSW_Test) or 0.4 to 1.2 Hz (HF_SSW_Test) was employed, while recorded acceleration data were used in the HF_CAM_Test and LF_CAM_Test. In the latter case, the selected Campano Lucano waveform was compressed in time by a factor of $\sqrt{3}$ to satisfy the 1/3 similitude criterion and scaled in amplitude to the Peak Ground Acceleration (PGA) level of 0.35 g The resulting ground acceleration histories measured by the accelerometer on the shake table in the various tests are illustrated in Figures 7 – 9.

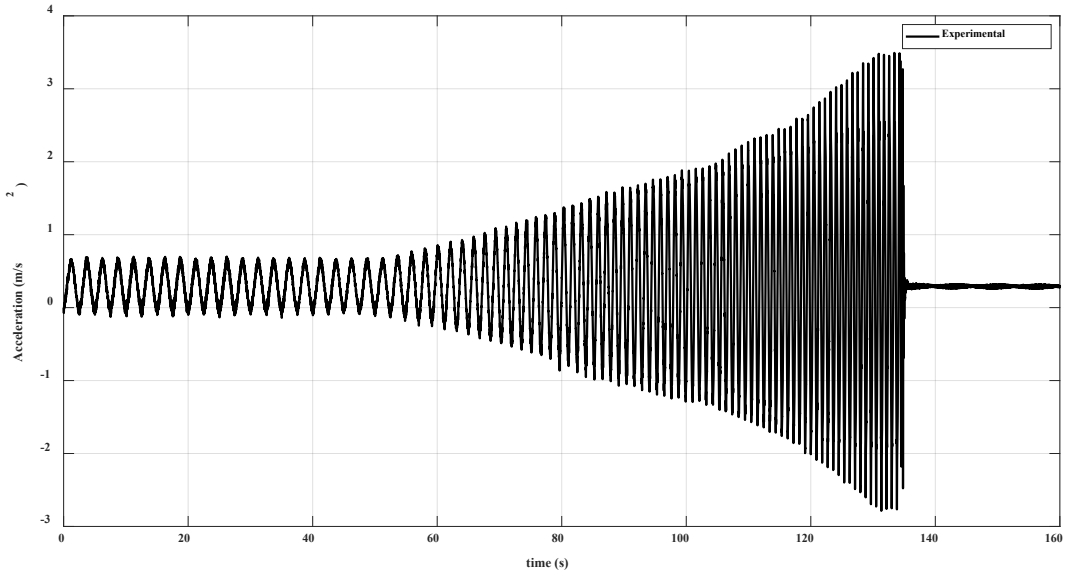


Figure 7. Shake table ground acceleration in HF_SSW_Test.

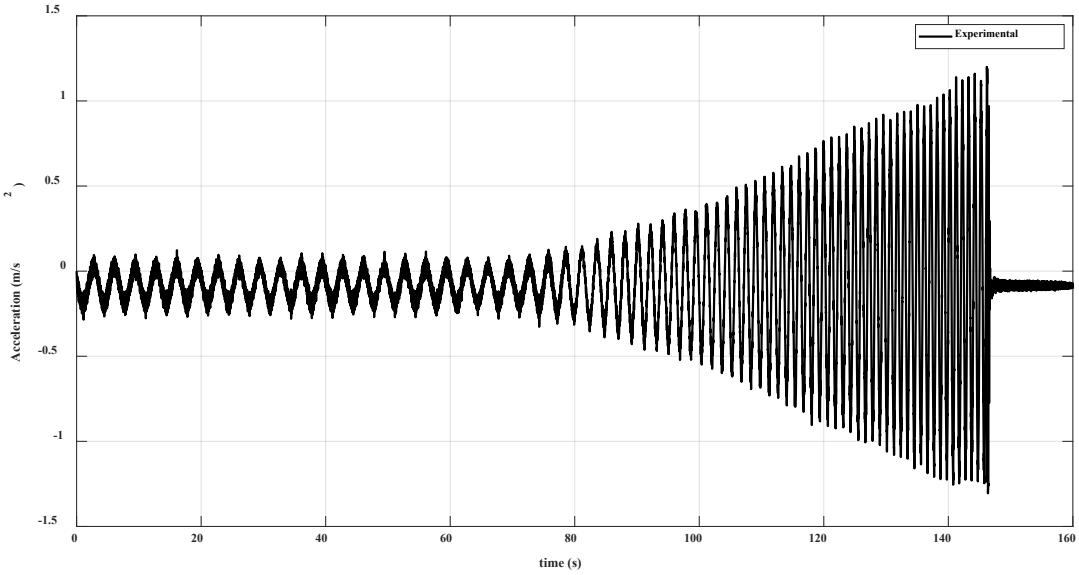


Figure 8. Shake table ground acceleration in LF_SSW_Test.

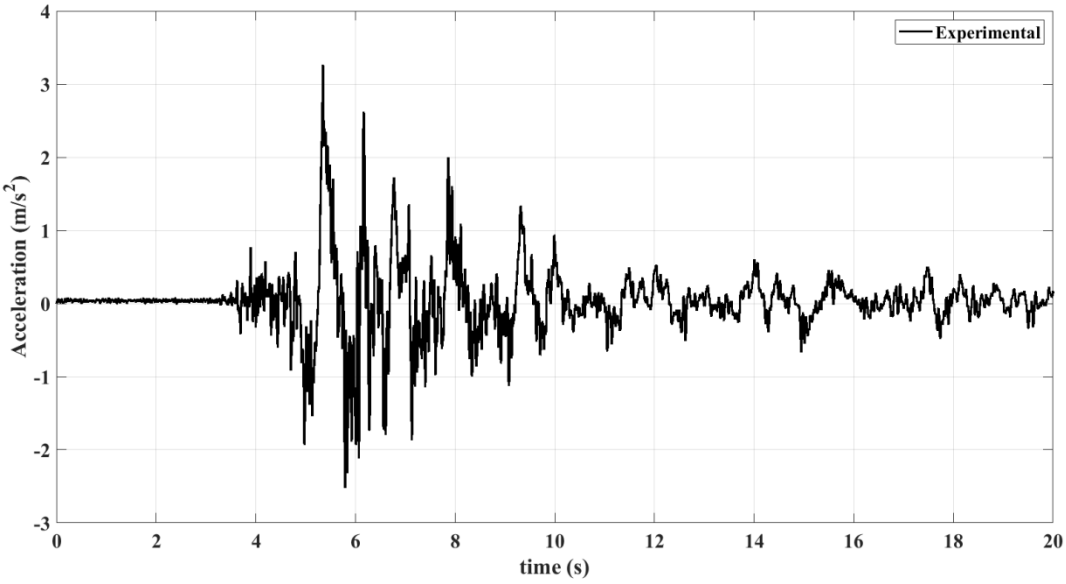


Figure 9. Shake table ground acceleration in HF_CAM_Test and LF_CAM_Test.

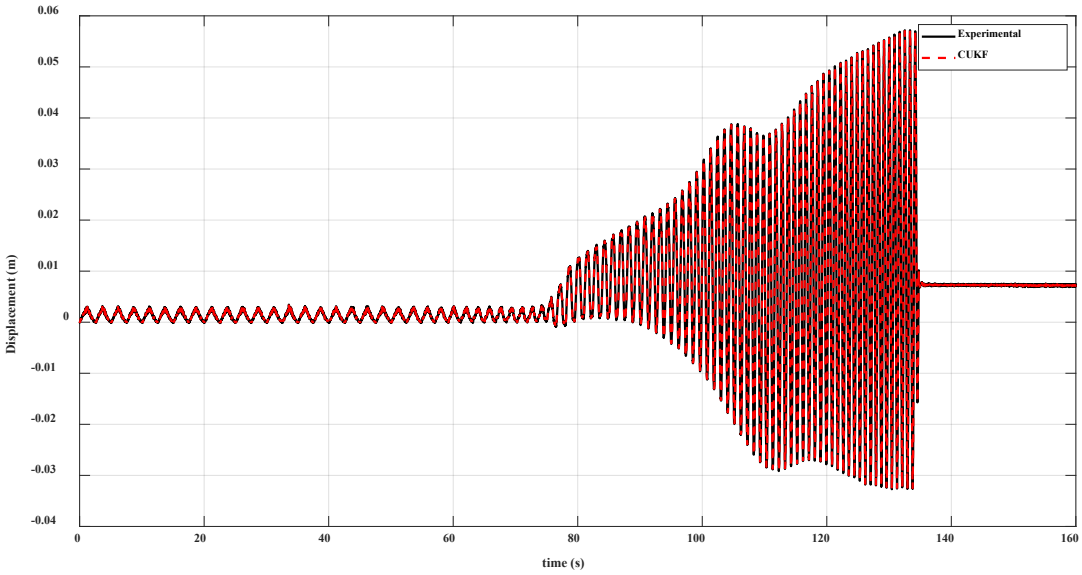
The base displacement of the structure relative to the shake table (the ground) is obtained by combining the absolute base and ground measurements provided by the sensors. For all tests, the CUKF was parametrized with a fixed time step of 0.001 s. The initial system state was set to $\boldsymbol{x} = [0,0,0,0,0,1]^T$, and the tuning parameter κ was set to 0. The model parameters are provided in Table 2.

Parameter	Unit	Value	
		HF	LF
m_b	Kg	3571	3571
m_t	Kg	4155	4155
k_s	N/m	1845000	1845000
c_s	Ns/m	5253	5253
R_c	m	1.485	1.485
n_i	-	4	4
μ_B	-	0.3	0.14
μ_{HV}	-	0.265	0.039
μ_{LV}	-	0.032	0.008
α_{dyn}	s/m	2	3
α_{St}	s/m	2	3

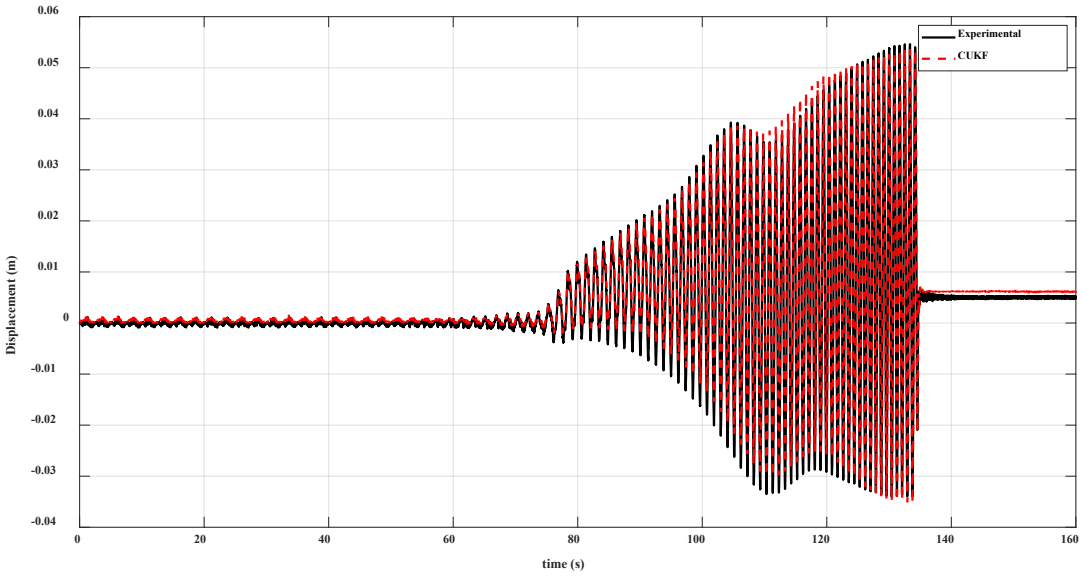
Table 2**.** Model parameters – Experimental Tests

4.1 Sine sweep test in high friction condition (HF_SSW_Test)

In this test, the process noise covariance and measurement noise covariance matrix were assumed as $\mathbf{Q} = diag(0.5 \cdot 10^{-9}, 10^{-10}, 0.5 \cdot 10^{-9}, 10^{-10}, 10^{-20}, 10^{-11})$ and $R = 10^{-12}$. In order to improve the identification and the estimation of the hysteretic degradation function, a set of constraints were applied at the estimated states. The upper constraints were $\boldsymbol{x_U} = [\infty, \infty, \infty, \infty, \infty, 1]$ while the lower constraints were $\boldsymbol{x_L} = [-\infty, -\infty, -\infty, -\infty, -\infty, 0]$. Figures 10(a) and 10(b) compare the experimental displacement histories at base and top levels of the structure to the ones provided by the CUKF.



(a)



(b)

Figure 10. HF_SSW_Test: Estimation of structure bottom (a) and top (b) displacement histories

At the start of the test, until 76 s, the ground acceleration is at the base level (0.4 m/s^2, Figure 7) and it's not sufficient to trigger the sliding of the isolators, which remain in their sticking condition. Therefore, only small displacements produced from the elastic deflection of the structure are observed. Since in this stage sliding is not engaged, the hysteretic friction degradation is null. At about 80 s, the ground acceleration starts to grow linearly according to the sweep modulation. Sliding

at the isolators' interfaces is triggered and the displacements at top and base levels increase, reaching peak values on the order of 50 mm at the resonance frequency.

The CUKF is indeed able to estimate the displacement histories, with small deviations on the peak displacements on the order of 5 mm. After about 134 s, the excitation is stopped. The high friction at small speeds prevented the complete re-centring of the structure and a residual displacement on the order of 7 mm was recorded (Fig. 10(a)), and consistently estimated by the CUKF.

The estimated history of the hysteretic degradation function is shown in Figure 11. A random walk model approach (RWM) is employed to identify this function with a *priori* no knowledge of a specific analytical formulation. Only the time window from 90 s to 134 s, when sliding of the isolators is engaged, is selected to provide this estimation.

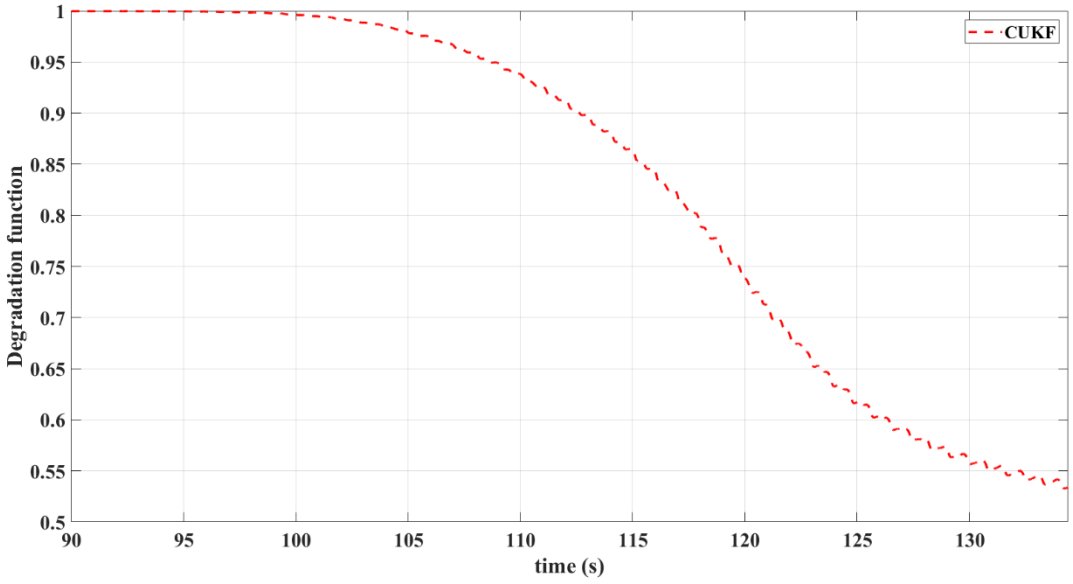


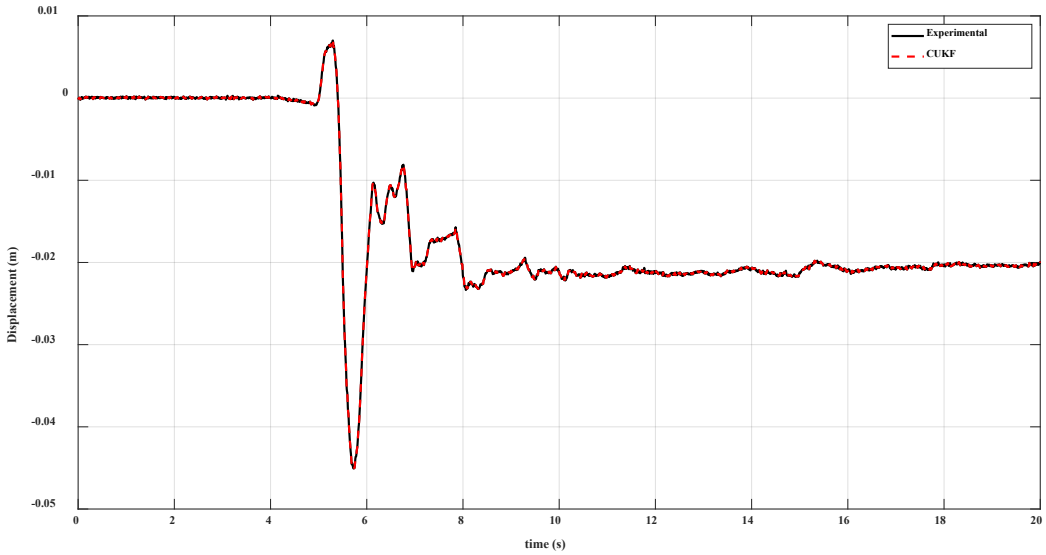
Figure 11. HF_SSW_Test: Estimation of hysteretic friction degradation function

The value of the hysteretic degradation function decreases from unity, as sliding starts, to 0.54 at the end of the excitation, after 134 s. It is possible to identify three distinct phases: (a) in the early stages of the excitation, till 110 s, the rate of deterioration (i.e. the slope of the curve) increases as the input frequency (and consequently the sliding velocity) of the CSSs increase; (b) at about 110 s the rate of deterioration reaches a maximum value, and then holds constant up to 125 s; (c) beyond 125 s the rate of deterioration decreases though the frequency and the sliding velocity increase. From a physical point, the increase in sliding velocity produces an increase in the dissipated energy and therefore of the temperature at the sliding surface, which in turn promotes a decrease in the coefficient of friction. However, a lower value of the coefficient of friction reduces the dissipation capability of the system,

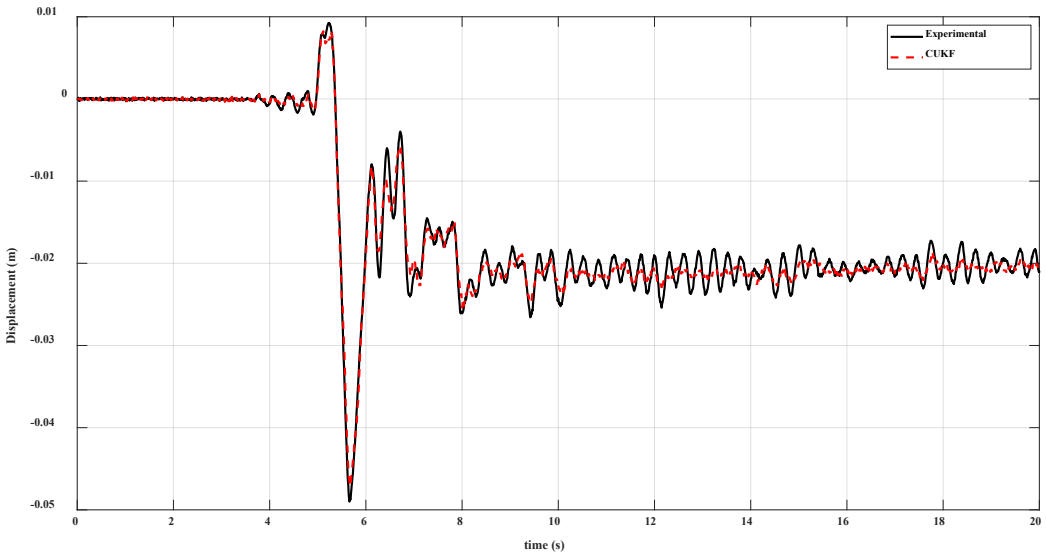
and therefore the hysteretic degradation rate, till a steady state is eventually reached, according to a mechanism of "thermal control of friction" [46].

4.2 Campano-Lucano test in high friction condition (HF_CAM_Test)

In this test, the process noise covariance and measurement noise covariance matrix were assumed as $\mathbf{Q} = diag(10^{-7},10^{-10},10^{-7},10^{-10},10^{-9},10^{-8})$ and $\mathrm{R} = 10^{-12}$. The upper constraints $\boldsymbol{x_U} = [\infty, \infty, \infty, \infty, \infty, 1]$ and the lower constraint $\boldsymbol{x_L} = [-\infty, -\infty, -\infty, -\infty, -\infty, 0]$ were applied to the estimated states. Figures 12(a) and 12(b) compare the experimental displacement histories at the base and top levels of the structure to the ones provided by the CUKF.



(a)



(b)

Figure 12. HF_CAM_Test: Estimation of structure base (a) and top (b) displacement histories

Some small elastic vibrations of the structure are observed at the early stages of the test when the base acceleration level is low; eventually at 5 s an acceleration spike of more than 2 m/s^2 occurs and sliding at the isolators' interfaces is triggered. The maximum displacements measured at both top and base levels are of the order of 45 mm.

The CUKF estimator is able to track correctly the experimental displacement histories at both base and top levels during the strong motion stage. After about 8 s, the acceleration drops to low levels, sliding of the isolator stops and the structure again develops small elastic deformations. The measured base displacement at the end of coda is of the order of 20 mm, correctly estimated by the CUKF, whereas some small oscillations about the experimental value are predicted at the top level which are ascribed to both the unmodelled dynamics in the model for the CUKF synthesis, and the effect of the experimental bias contained in the input acceleration.

The estimation of the hysteretic degradation function is shown in Figure 13, where only the time frame from 5 to 7 s is considered.

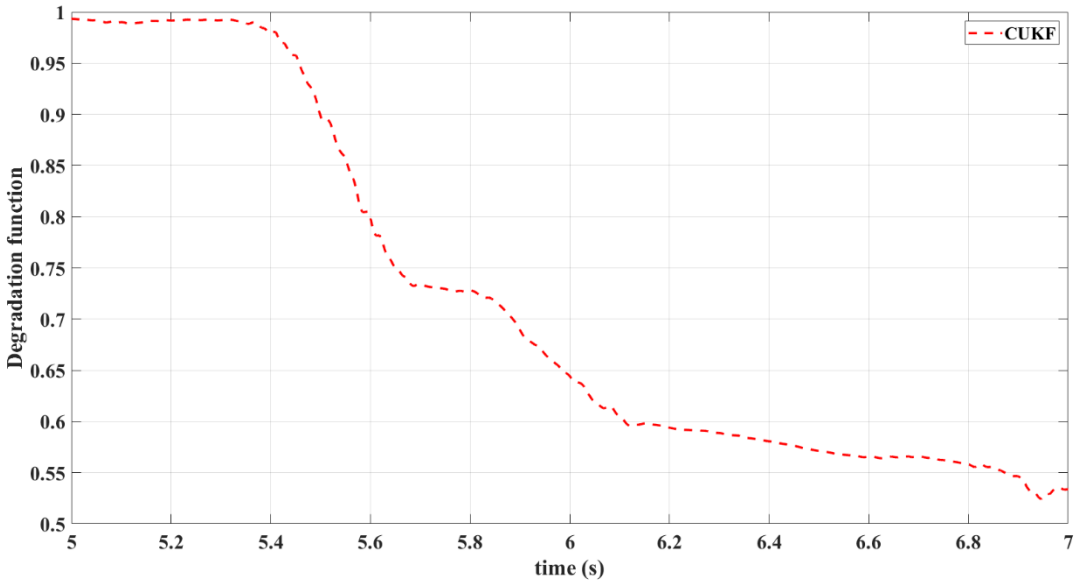
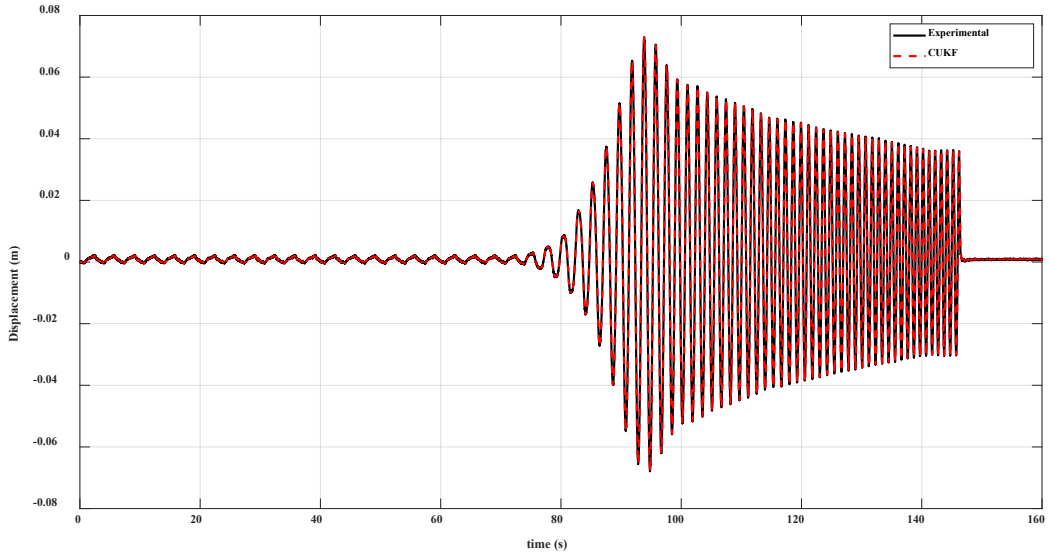


Figure 13. HF_CAM_Test: Estimation of friction degradation function

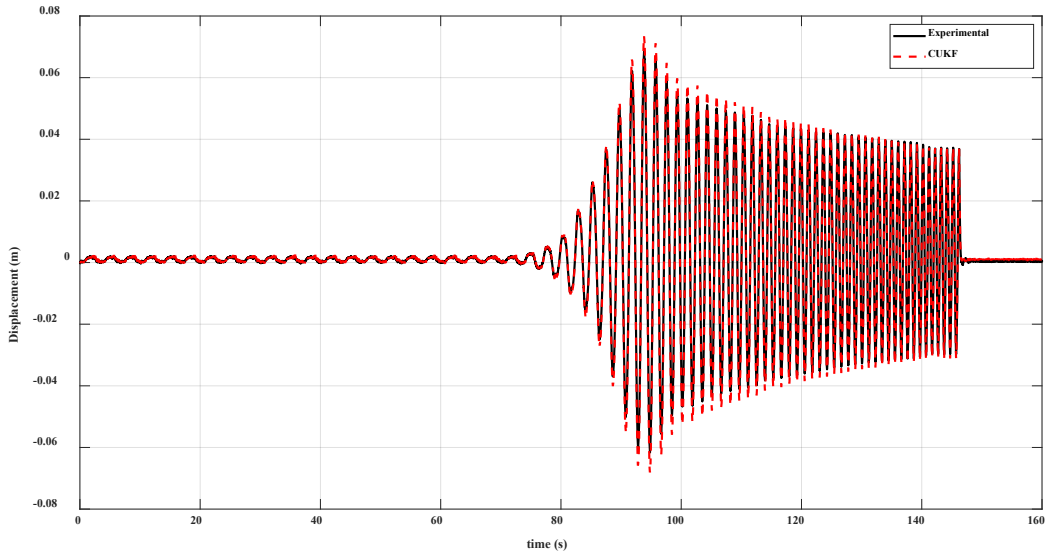
In the time window [5 s, 7 s], the relative velocities and displacements at the isolators' sliding surfaces caused by the seismic input are large, and therefore the energy dissipation and the relevant friction degradation are very important. A 47% degradation of the coefficient of friction is estimated to occur for the high friction material, with the largest part (about 40%) taking place from 5.4 to 6.1 s in correspondence of the largest displacements.

4.3 Sine sweep test in low friction condition (LF_SSW_Test)

The process noise covariance and measurement noise covariance matrix were assumed as $\mathbf{Q} = diag(10^{-11},10^{-14},10^{-11},10^{-14},10^{-20},10^{-15})$ and $\mathrm{R} = 10^{-16}$. The upper constraints $\boldsymbol{x_U} = [\infty, \infty, \infty, \infty, \infty, 1]$ and the lower constraint $\boldsymbol{x_L} = [-\infty, -\infty, -\infty, -\infty, -\infty, 0]$ were applied to the estimated states. Figures 14(a) and 14(b) compare the experimental displacement histories at the base and top levels of the structure to the ones provided by the CUKF.



(a)



(b)

Figure 14. LF_SSW_Test: Estimation of structure base (a) and top (b) displacement histories

Sliding of the isolators is triggered at approximately 80 s. The maximum displacements at both top and base levels are developed at about 95 s when resonance is reached, and then decrease as the frequency is further increased. The CUKF estimations of base and top frame displacements correctly follow the experimental histories. The permanent base displacement at the end of the test is negligible (less than 1 mm). The estimation of the hysteretic degradation function is shown in Figure 15. Only the time window from 80 s to 148 s when sliding is actually engaged is selected to provide this estimation

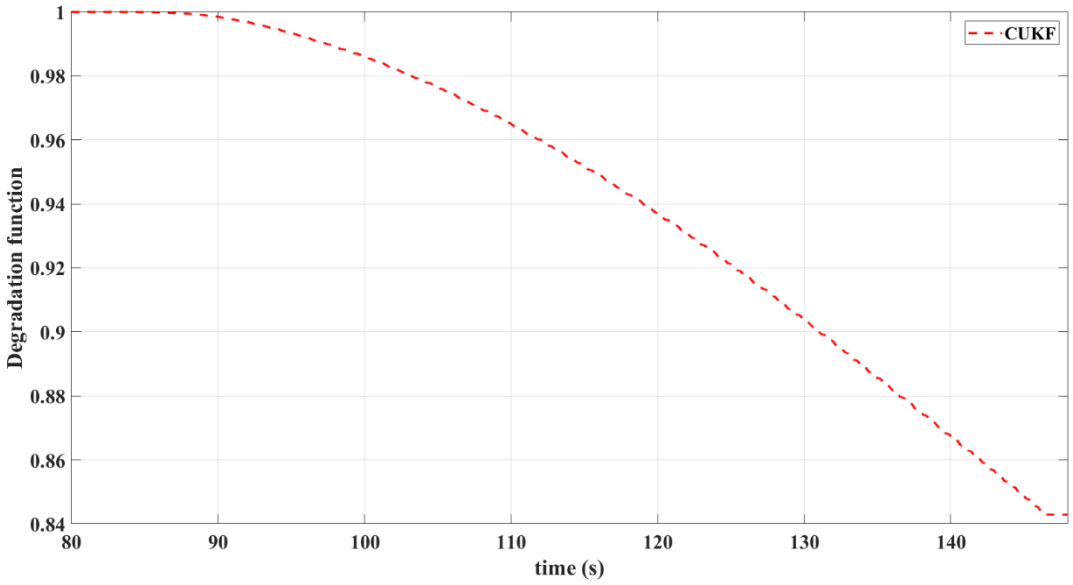
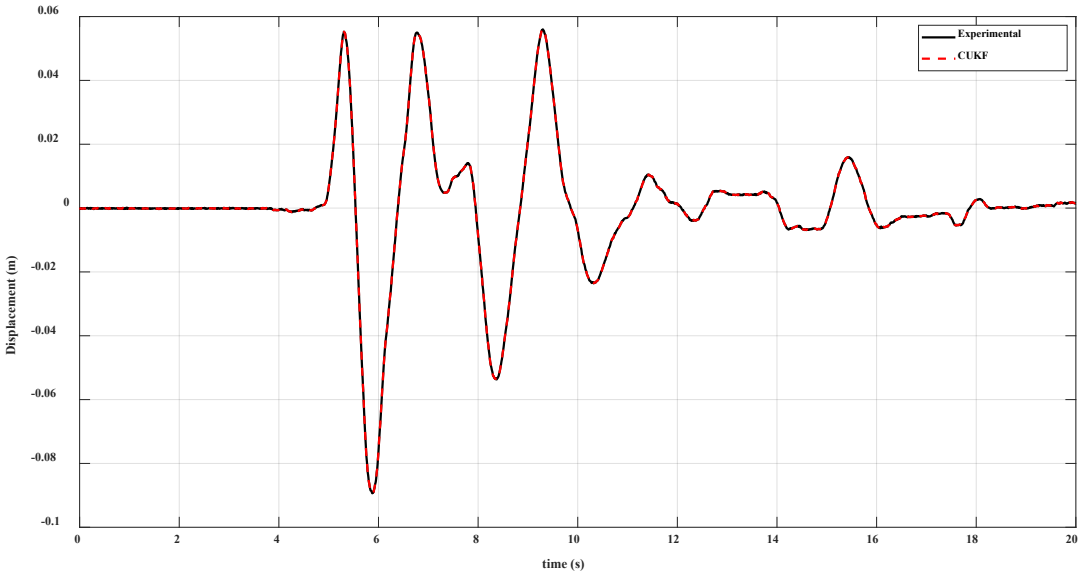


Figure 15. LF_SSW_Test: Estimation of friction degradation function

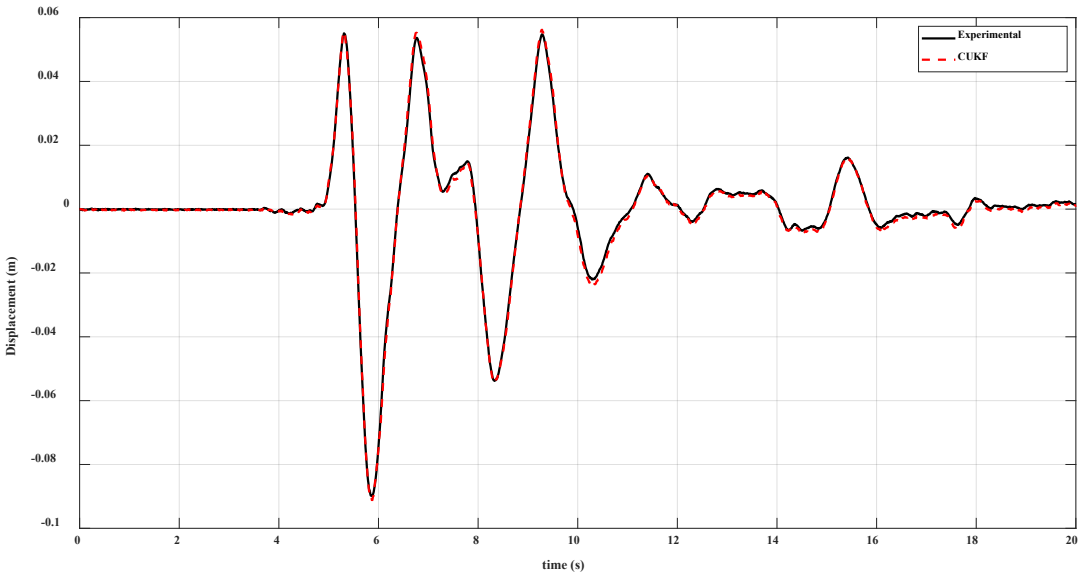
Over the considered time interval, the hysteretic degradation in low friction condition is on the order of 15%, significantly smaller than that observed (47%) in high friction condition, because of the smaller energy dissipation and heat generation at the sliding surface. It is interesting to compare the different histories of the degradation function f_c shown in Figure 11 and Figure 15. In contrast to the sigmoidal shape of f_c identified for the HF material and discussed earlier, for the LF material the rate of degradation is almost constant for increasing frequencies. This different behaviour is an effect of the different dissipation capacities associated to either high or low friction coefficient; the lower energy dissipation induces a smaller temperature rise and therefore for the LF material the constant temperature regime is far from being reached over the duration of the test; therefore the coefficient of friction continuously decreases with increasing speed. In contrast, for the HF material the decreasing rate of degradation at high frequencies indicates that owing to the large energy dissipation the system is approaching the thermal equilibrium condition and the coefficient of friction is approaching its lower bound value.

4.4 Campano-Lucano test in low friction condition (LF_CAM_Test)

The process noise covariance and measurement noise covariance matrix were assumed as $\mathbf{Q} = diag(10^{-11},10^{-14},10^{-11},10^{-14},10^{-20},10^{-13})$ and $\mathrm{R} = 10^{-16}$. The upper constraints $\boldsymbol{x_U} = [\infty, \infty, \infty, \infty, \infty, 1]$ and the lower constraint $\boldsymbol{x_L} = [-\infty, -\infty, -\infty, -\infty, -\infty, 0]$ were applied to the estimated states. Figures 16(a) and 16(b) compare the experimental displacement histories at the base and top levels of the structure to the ones provided by the CUKF.



(a)



(b)

Figure 16. LF_CAM_Test: Estimation of structure base (a) and top (b) displacement histories

Sliding of the isolators is engaged at about 5 s, when the acceleration peak of more than 2 m/s^2 is imposed to the shake table. The maximum displacements measured at both top and base levels are of the order of 90 mm. At about 11 s, the acceleration drops to low levels, sliding stops and the structure exhibits small elastic vibrations. Also in this case the CUKF estimates accurately the displacement histories of both base and top levels. The measured base displacement at the end of coda is of the order of 1 mm, as correctly predicted from the CUKF.

The estimation of the friction degradation function over the time interval from 5 to 11 s is shown in Figure 17.

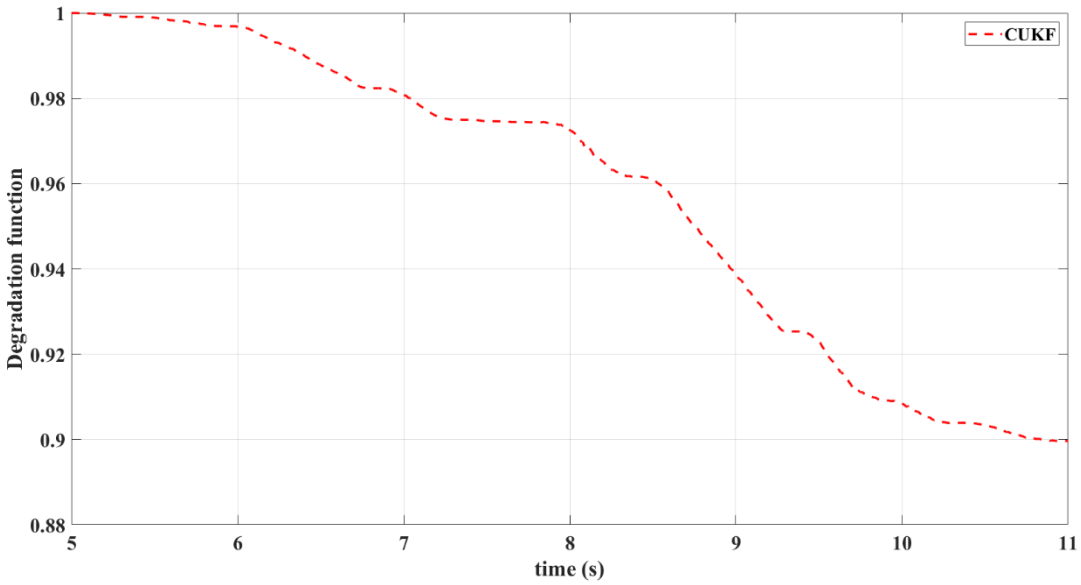


Figure 17. LF_CAM_Test: Estimation of friction degradation function

The hysteretic degradation function decreases from unity to 0.9 at the end of the excitation, involving a 10% change in the coefficient of friction. This change is about one fifth of the one estimated for the HF material under the application of the same ground motion acceleration history, and is justified by substantially smaller coefficient of friction, and hence damping capacity, of the LF material. It is also noticeable that the degradation of the coefficient of friction is now spread over a length of about 4 s (from 6 to 10 s) in comparison to about 0.7 s for the HF material, due to a longer sliding phase in low friction condition.

5. Conclusions

One of the issues in determining the design characteristics of curved surface sliders is represented by the estimation of the hysteretic degradation of the coefficient of friction consequent to the heating of the sliding surfaces. Though provisions have been recently introduced in codes [25], the lack of validated physical models hampers the interpretation of the experimental data and the formulation of accurate numerical models.

The study presents a novel estimator for the degradation of the coefficient of friction based on an Constrained Unscented Kalman Filter (CUKF) combined with a Random Walk Model approach (RWM) which identifies the friction degradation function without no a priori knowledge of a specific physical model and ensuing analytical law.

A benchmark model-based estimator for shear-type frames subjected to ground motion accelerations has been implemented and assessed by means of numerical simulations and experimental data.

The CUKF demonstrated, through numerical and experimental tests, to provide an accurate estimation of the state of the system, by predicting the structural displacement histories, and to identify the hysteretic degradation function in different friction conditions.

The CUKF estimator uses as input data the displacement histories of the isolators. In a practical application it could be fed with data collected during real-time monitoring of base isolated structures, to estimate the actual degradation of the coefficient of friction of the isolators during an earthquake, as a mean to verify the suitability of the lower bound friction coefficients adopted in structural design.

In the present study the CUKF was assessed over unidirectional data already available to the Authors. However, in a future study it will be applied to bidirectional data in order to assess its performance over more realistic ground motion histories.

References

[1] Zayas, V.A., Low, S.S., Mahin, S.A. (1987). The FPS Earthquake Protection System. Report No. 87-01. Earthquake Engineering Research Center, Berkeley.

[2] Zayas, V.A., Low, S.S., Mahin, S.A. (1990). A simple pendulum technique for achieving seismic isolation. Earthquake Spectra, **6**(2): 317-333.

[3] Quaglini, V., Gandelli, E., and Dubini, P. (2017) Experimental investigation of the re-centring capability of curved surface sliders, Struct. Control Health Monit., 24: e1870. doi: 10.1002/stc.1870.

[4] Quaglini, V, Gandelli, E, Dubini, P, Limongelli, MP. "Total displacement of curved surface sliders under nonseismic and seismic actions: A parametric study". Struct Control Health Monit. 2017; 24:e2031. https://doi.org/10.1002/stc.2031

[5] Martelli, A., Clemente, P., De Stefano, A., Forni, M., Salvatori, A. (2014) Recent development and application of seismic isolation and energy dissipation and conditions for their correct use. In: Ansal, A. Perspectives on European Earthquake Engineering and Seismology. Volume 1. Springer, New York, 449-488.

[6] Quaglini V. (2012) High damping curved surface sliding isolators for bridges. In: Biondini, F., Frangopol, D.M., editors. Bridge Maintenance, Safety, Management, Resilience and Sustainability. CRC Press, Boca Raton.

[7] Ponzo et al. (2015). Shaking table tests of a base isolated structure with double concave friction pendulum bearings. Bulletin of the New Zealand Society for Earthquake Engineering, Vol. 48(2), Pages 136-144

[8] Ponzo, F.C., Di Cesare, A., Leccese, G., Nigro, D. (2017) Shake table testing on restoring capability of double concave friction pendulum seismic isolation systems, Earthquake Engineering and Structural Dynamics, Vol.46(14), Pages 2337-2353

[9] Ragni, L., Cardone, D., Conte, N., Dell´Asta, A., Di Cesare A., Flora, G., Leccese, G., Micozzi, F., Ponzo, C. (2018). Modelling and Seismic Response Analysis of Italian Code-Conforming Base-Isolated Buildings. Journal of Earthquake Engineering, Vol. 22-sup2, Pages 198-230

[10] Cardone, D.; Conte, N.; Dall'Asta, A.; Di Cesare, A.; Flora, A.; Leccese, G.; Micozzi, F.; Ponzo, F.; Ragni, L. (2019). RINTC-E project: The seismic risk of existing Italian RC buildings retrofitted with seismic isolation. Compdyn 2019 proceedings, Crete, Greece

[11] Ponzo, F.C., Di Cesare, A., Leccese, G., Nigro, D. (2019). Standard requirements for the recentring capability of curved surface sliders. Ingegneria Sismica

[12] CEN (2004) Eurocode 8: Design of structures for earthquake resistance—Part 1: General rules, seismic actions and rules for buildings, EN1998‑1:2004. European Committee for Standardization, Bruxelles, Belgium.

[13] CEN (2005) Eurocode 8: Design of structures for earthquake resistance—Part 2: Bridges, EN1998-EN1998‑2:2005+A1:2011. European Committee for Standardization, Bruxelles, Belgium.

[14] Lomiento, G., Bonessio, N., Benzoni, G. (2013). Friction model for sliding bearings under seismic excitation. Journal of Earthquake Engineering, **17**(8): 1162-1191.

[15] Constantinou, M.C., Whittaker, A.S., Kalpakidis, Y., Fenz, D.M., Warn, G.P. (2007). Performance of Seismic Isolation Hardware under Service and Seismic Loading. Report MCEER-07-0012. National Center for Earthquake Engineering Research, Buffalo.

[16] Quaglini, V., Bocciarelli, M., Gandelli E., Dubini, P. (2014) "Numerical Assessment of Frictional Heating in Sliding Bearings for Seismic Isolation", Journal of Earthquake Engineering, Vol. 18(8), pp. 1198-1216, DOI: 10.1080/13632469.2014.924890

[17] Emanuele Gandelli & Virginio Quaglini (2018) Effect of the Static Coefficient of Friction of Curved Surface Sliders on the Response of an Isolated Building, Journal of Earthquake Engineering, DOI: 10.1080/13632469.2018.1467353

[18] Mosqueda, G., Whittaker, A. S. and Fenves, G. L. [2004] "Characterization and modeling of friction pendulum bearings subjected to multiple components of excitation," Journal of Structural Engineering ASCE 130(3), 433–442. doi:10.1061/(ASCE)0733-9445(2004)130:3(433).

[19] Lomiento, G., Bonessio, N., Benzoni, G. (2013). Concave sliding isolator's performance under multi-directional excitation. Ingegneria Sismica., 30(3): 17-32.

[20] Quaglini, V., Dubini, P. & Poggi, C. Experimental assessment of sliding materials for seismic isolation systems. Bull Earthquake Eng 10, 717–740 (2012). https://doi.org/10.1007/s10518-011-9308-9

[21] Kumar, M., Whittaker, A.S., Constantinou, M.C. (2015). Characterizing friction in sliding isolation bearings. Earthquake Engineering and Structural Dynamics, **44**(9): 1409-1425.

[22] Gandelli, E., Penati, M., Quaglini, V., Lomiento, G., Miglio, E., Benzoni, G.M. (2019). A novel OpenSees element for single curved surface sliding isolators. Soil Dynamics and Earthquake Engineering, **119**(4): 433-453.

[23] Gandelli, E., Quaglini, V., Dubini, P., Limongelli, M. P., & Capolongo, S. (2018). Seismic isolation retrofit of hospital buildings with focus on non-structural components. http://hdl.handle.net/11311/1072414.

[24] Marco Furinghetti, Alberto Pavese, Virginio Quaglini, Paolo Dubini (2019). Experimental investigation of the cyclic response of double curved surface sliders subjected to radial and bidirectional sliding motions, Soil Dynamics and Earthquake Engineering, Volume 117,2019, Pages 190-202,ISSN 0267-7261,https://doi.org/10.1016/j.soildyn.2018.11.020.

[25] ASCE, American Society of Civil Engineers (2017). Minimum Design Loads and Associated Criteria for Buildings and Other Structures ASCE/SEI 7-16, doi: 10.1061/9780784414248.

[26] AASHTO, American Association of State Highway and Transportation Officials (1999). Guide Specification for Seismic Isolation Design. Washington D. C.

[27] CEN - Comité Européen de Normalisation (2009). EN15129 - Antiseismic Devices. Brussels, Belgium

[28] Salvatore Strano, Mario Terzo, Constrained nonlinear filter for vehicle sideslip angle estimation with no a priori knowledge of tyre characteristics, Control Engineering Practice, Volume 71, 2018, Pages 10-17.

[29] Calabrese A, Strano S, Terzo M. Adaptive constrained unscented Kalman filtering for real-time nonlinear structural system identification. Struct Control Health Monit. 2018;25:e2084. https://doi.org/10.1002/stc.2084

[30] Ingo Kaiser, Salvatore Strano, Mario Terzo, Ciro Tordela, Anti-yaw damping monitoring of railway secondary suspension through a nonlinear constrained approach integrated with a randomly variable wheel-rail interaction, Mechanical Systems and Signal Processing, Volume 146, 2021, 107040, ISSN 0888-3270, https://doi.org/10.1016/j.ymssp.2020.107040.

[31] Kolas, S., Foss, B., & Schei, T. (2009). Constrained nonlinear state estimation based on the UKF approach. *Computers & Chemical Engineering*, *33*(8), 1386–1401.

[32] Mandela, R., Kuppuraj, V., Rengaswmy, R., & Narasimhan, S. (2012). Constrained unscented recursive estimator for nonlinear dynamic systems. *Journal of Process Control*, *22*(4), 718–728.

[33] Julier, S., Uhlmann, J., & Durrant-Whyte, H. F. (2000). A new method for the nonlinear transformation of means and covariances in filters and estimators. IEEE Transactions on Automatic Control, 45(3), 477-482. doi:10.1109/9.847726

[34] B. Wu, T. Wang, Model updating with constrained unscented Kalman filter for hybrid testing, Smart Structures and Systems. 14 (6), (2014) 1105-1129.

[35] Calabrese A, Quaglini V, Strano S, Terzo M. Online estimation of the friction coefficient in sliding isolators. Struct Control Health Monit. 2019;e2459. https://doi.org/10.1002/stc.2459

[36] Niola, V., Strano, S., and Terzo, M. (March 27, 2018). "A Random Walk Model Approach for the Wheel-Rail Contact Force Estimation." ASME. *J. Dyn. Sys., Meas., Control*. July 2018; 140(7): 071016.

[37] Simon, D. (2006). Optimal State Estimation: Kalman, H Infinity, and Nonlinear Approaches. John Wiley and Sons Inc.

[38] Naeim, F., Kelly, J. M. (1999) “Design of Seismic Isolated Structures, From Theory to Practice”, John Wiley and Sons, ISBN 0-471-14921-7

[39] Al-Hussaini, T. M., Zayas, V. A. and Constantinou, M. C. 1994 “Seismic isolation of multi-story frame structures using spherical sliding isolation systems,” Report No. NCEER-94-0007, National Center for Earthquake Engineering Research, Buffalo.

[40] McKenna F., Fenves G.L., Scott, M.H., Jeremic, B. (2000). Open System for Earthquake Engineering Simulation (OpenSees). Pacific Earthquake Engineering Research Center (PEER), Berkeley, USA

[41] OpenSeesWiki, online manual, available at: http://opensees.berkeley.edu/wiki/index.php/Main_Page

[42] Calabrese, A., Spizzuoco, M.C., Serino, G., Della Corte, G., Maddaloni, G. (2015). Shaking table investigation of a novel, low-cost, base isolation technology using recycled rubber. Structural Control and Health Monitoring, Vol. 22(1), pp. 107-122, DOI: 10.1002/stc.1663.

[43] Fenz, D.M., Constantinou, M.C. (2006). Behaviour of the double concave Friction Pendulum bearing. Earthquake Engineering and Structural Dynamics, Vol. 35(11), pp. 1403-1424, DOI: 10.1002/eqe.589.

[44] Quaglini V, Dubini P, Poggi C. (2012). Experimental assessment of sliding materials for seismic isolation systems. Bulletin of Earthquake Engineering; Vol. 10(2), Pages 717–740. doi:10.1007/s10518-011-9308-9

[45] Ambraseys, N., Smit, P., Sigbjornsson, R., Suhadolc, P., Margaris, B. (2002) http://www.isesd.cv.ic.ac.uk/ESD/ Internet-Site for European Strong-Motion Data, European Commission, Research-Directorate General, Environment and Climate Programme.

[46] Virginio Quaglini, Paolo Dubini, Daniela Ferroni, Carlo Poggi, Influence of counterface roughness on friction properties of engineering plastics for bearing applications, Materials & Design, Volume 30, Issue 5, 2009, Pages 1650-1658, ISSN 0261-3069, https://doi.org/10.1016/j.matdes.2008.07.025.